Anomalous finite-size effect due to quasidegenerate phases in triangular antiferromagnets with long-range interactions and mapping to the generalized six-state clock model

Masamichi Nishino[1,*] and Seiji Miyashita[2]

[1]*National Institute for Materials Science, Tsukuba, Ibaraki 305-0047, Japan*

[2]*Department of Physics, Graduate School of Science, The University of Tokyo, Bunkyo-Ku, Tokyo, Japan*

(Received 8 August 2016; revised manuscript received 4 October 2016; published 28 November 2016)

The effect of long-range (LR) interactions on frustrated-spin models is an interesting problem, which provides rich ordering processes. We study the effect of LR interactions on triangular Ising antiferromagnets with the next-nearest-neighbor ferromagnetic interaction (TIAFF). In the thermodynamic limit, the LRTIAFF model should reproduce the corresponding mean-field results, in which successive phase transitions occur among various phases, i.e., the disordered paramagnetic phase, so-called partially disordered phase, three-sublattice ferrimagnetic phase, and two-sublattice ferrimagnetic phase. In the present paper we focus on the magnetic susceptibility at the transition point between the two-sublattice ferrimagnetic and the disordered paramagnetic phases at relatively large ferromagnetic interactions. In the mean-field analysis, the magnetic susceptibility shows no divergence at the transition point. In contrast, a divergencelike enhancement of the susceptibility is observed in Monte Carlo simulations in finite-size systems. We investigate the origin of this difference and find that it is attributed to a virtual degeneracy of the free energies of the partially disordered and 2-FR phases. We also exploit a generalized six-state clock model with an LR interaction, which is a more general system with Z_6 symmetry. We discuss the phase diagram of this model and find that it exhibits richer transition patterns and contains the physics of the LRTIAFF model.

DOI: 10.1103/PhysRevB.94.184434

I. INTRODUCTION

The effect of frustration brings a variety of critical phenomena and phase transitions [1]. The triangular Ising antiferromagnet is a typical example [2–4]. It exhibits a critical point only at zero temperature, where the system has macroscopic degeneracy. The $CsCoCl_3$ is an experimental counterpart, which is a three-dimensional (3D) system with layered triangular lattices and exhibits successive phase transitions [5].

Taking into account a strong interlayer coupling, Mekata modeled the system by the triangular Ising antiferromagnet with a next-nearest-neighbor ferromagnetic (TIAFF) interaction and analyzed it by a mean-field (MF) method [6]. He found that there exist various interesting phases: disordered (D), partially disordered (PD), three-sublattice ferrimagnetic (3-FR), and two-sublattice ferrimagnetic (2-FR) phases. When the ratio α (>0) [7] between the nearest-neighbor (NN) antiferromagnetic coupling and the next-nearest-neighbor (NNN) ferromagnetic coupling is lower than a critical value (case I: $\alpha < \alpha_C$), successive phase transitions take place among them. When the ratio is higher (case II: $\alpha > \alpha_C$), the D phase changes to the 2-FR phase directly, and vice versa.

Since the prediction of the PD phase attracted much interest, many studies of the TIAFF model by Monte Carlo (MC) methods have been performed to clarify the nature of the phase [8–11]. On the other hand, the TIAFF model has been intensively studied to elucidate the multicritical behavior of lattice gas models because under a magnetic field it is equivalent to a triangular lattice gas model which describes, in particular, the adsorption of helium on graphite [12–14].

Those studies reached the consensus that in two dimensions, the TIAFF model exhibits double Berezinskii-Kosterlitz-Thouless (BKT) transitions [15,16]. The model has been analyzed by mapping from the Ising configuration on a triangular lattice to the six-state clock (6SC) modes [8–11,13,17], and the nature of phase transitions of the systems which pose Z_6 symmetry has been studied [18–20]. Between the BKT critical points a characteristic intermediate-temperature phase exists, in which the correlation function decays with a power law $r^{-\eta}$ with temperature-dependent exponent $\eta(T)$. Thus this phase is qualitatively different from the PD phase.

The PD phase was found between the 2-FR and the D phases in MC studies of the 3D model without [10,21,22] and with [23,24] the NNN interaction. A picture of the first-order phase transition between the 2-FR and the PD phases without latent heat has been proposed, which explains the experimental results of $CsCoCl_3$ [24]. The structure of the phase transitions has also been understood by the use of renormalization-group (RG) flow diagrams [21,24,25].

The importance of the long-range (LR) nature of the interaction has been suggested in spin-crossover compounds, which exhibit rich phase transitions by a variety of external perturbations, such as light, pressure, and magnetic field [26–54]. This feature has attracted much attention for applications to photomemory, sensors, etc.

It has been pointed out that the effective LR interaction is realized by elastic interactions [45,51,52]. Recently we studied the effect of the LR interaction on the TIAFF model for spin crossover and found that the double BKT transitions are modified to a combination of a second-order transition with a new critical universality (low-temperature end point) and a BKT transition (high-temperature end point) [54]. There the elastic interaction plays as an infinite-range interaction among all sites.

The infinite-range interaction has been used as a theoretical tool to study the properties of the LR interaction in the

*Corresponding author: nishino.masamichi@nims.go.jp

strong limit and equivalence to the MF model, but now it is a practical one.

Furthermore, recently the difference in transition properties between finite size (nano) and bulk in spin-crossover compounds has been in the limelight [55–59]. Namely, the effect of the LR interaction may be modified by the finite-size effect. Therefore, it is important to investigate both the effect of LR interactions and the finite-size effect.

In the present work we study antiferromagnetic intersublattice LR and ferromagnetic intrasublattice LR interactions acting on the three sublattices of the TIAFF model. This model corresponds to the above-mentioned Mekata's three-subalttice MF model in the thermodynamic limit. We focus on the finite-size effect. We call the TIAFF model with these sublattice long-range interactions the *long-range TIAFF* (LRTIAFF) model. In particular, we study case II ($\alpha > \alpha_C$).

The MF analysis shows that the magnetic susceptibility diverges only between the PD and the 3-FR phases in case I. However, we find that an unexpected divergencelike enhancement of the susceptibility of a different origin appears between the 2-FR and the D phases in case II in finite-size systems. We investigate the origin of this divergencelike behavior. It is found that the free energy has a peculiar structure and the difference in free energies between the PD and the 2-FR phases is very small, which causes a divergencelike enhancement of the magnetic susceptibility in MC simulations even in a large system.

Because the properties of the TIAFF model are well understood from the picture of the nonchiral 6SC model, we exploit a general and fundamental expression for the LRTIAFF model, which is called the long-range generalized six-state clock (LRG6SC) model. We demonstrate that the LRG6SC model has richer transition patterns and the LRTIAFF model is well captured in a part of the phase diagram of the LRG6SC model.

The rest of the paper is organized as follows. In Sec. II, the LRTIAFF model is introduced. In Sec. II A, we review properties of the LRTIAFF model in the thermodynamic limit. In Sec. II B, we give the method for study of finite-size effects of the LRTIAFF model and investigate the finite-size properties. Section III is devoted to study of the LRG6SC model in the thermodynamic limit and discussion of the phase diagram, including the correspondence between the LRTIAFF and the LRG6SC models. The finite-size effect in the LRG6SC model is summarized in Appendix A and the critical value of the control parameter for the LRG6SC model is given in Appendix B. In Sec. IV, we provide a discussion and summary.

II. TRIANGULAR ANTIFERROMAGNET WITH LONG-RANGE INTERACTIONS

The Hamiltonian of the TIAFF model is given by

$$\begin{aligned}\mathcal{H} = &-J_1 \sum_{\langle i,j\rangle} \sigma_i^{\mathrm{A}}\sigma_j^{\mathrm{B}} - J_1 \sum_{\langle i,j\rangle} \sigma_i^{\mathrm{B}}\sigma_j^{\mathrm{C}} - J_1 \sum_{\langle i,j\rangle} \sigma_i^{\mathrm{C}}\sigma_j^{\mathrm{A}} \\ &- J_2 \sum_{\langle\langle i,j\rangle\rangle} \sigma_i^{\mathrm{A}}\sigma_j^{\mathrm{A}} - J_2 \sum_{\langle\langle i,j\rangle\rangle} \sigma_i^{\mathrm{B}}\sigma_j^{\mathrm{B}} \\ &- J_2 \sum_{\langle\langle i,j\rangle\rangle} \sigma_i^{\mathrm{C}}\sigma_j^{\mathrm{C}} - h\sum_{i=1} \sigma_i, \end{aligned} \tag{1}$$

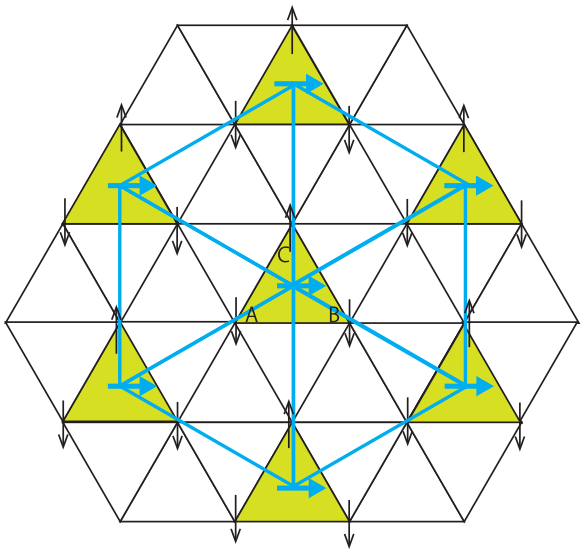

FIG. 1. Triangular lattice for the TIAFF model (black lattice) and that for the 6SC model (blue lattice). Each colored triangular plaquette (green) has three spins of sublattices A, B, and C. Spin configurations of the colored triangular plaquettes are mapped to spin states of the 6SC model [see Figs. 5 and 10(b)]. The spin configuration here corresponds to a ground-state configuration of the TIAFF model (black arrows) and the 6SC model (blue arrows) under zero field.

where each site belongs to sublattice A, B, or C, σ_i^{A} denotes the spin state at site i on sublattice A and takes 1 or -1, and σ_i^{B} and σ_i^{C} are defined in the same manner (Fig. 1). The antiferromagnetic intersublattice interaction and the ferromagnetic intrasublattice interaction are denoted $J_1 < 0$ and $J_2 > 0$, respectively, and h is a magnetic field. Here $\langle i,j\rangle$ and $\langle\langle i,j\rangle\rangle$ denote the NN and NNN couplings, respectively. The coordination number for the three J_2 terms is $z = 6$, while that for the three J_1 terms is $z/2 = 3$.

In the present work, we study a model of LR interactions for the TIAFF model (LRTIAFF model):

$$\begin{aligned}\mathcal{H} = &-\frac{J_1 z/2}{N/3}\sum_{i,j} \sigma_i^{\mathrm{A}}\sigma_j^{\mathrm{B}} - \frac{J_1 z/2}{N/3}\sum_{i,j} \sigma_i^{\mathrm{B}}\sigma_j^{\mathrm{C}} \\ &- \frac{J_1 z/2}{N/3}\sum_{i,j} \sigma_i^{\mathrm{C}}\sigma_j^{\mathrm{A}} - \frac{J_2 z}{N/3}\sum_{i<j} \sigma_i^{\mathrm{A}}\sigma_j^{\mathrm{A}} - \frac{J_2 z}{N/3}\sum_{i<j} \sigma_i^{\mathrm{B}}\sigma_j^{\mathrm{B}} \\ &- \frac{J_2 z}{N/3}\sum_{i<j} \sigma_i^{\mathrm{C}}\sigma_j^{\mathrm{C}} - h\sum_{i=1}^{N} \sigma_i, \end{aligned} \tag{2}$$

where the sum of the interactions is taken all over the pairs, N is the number of sites in the system, and the coefficient $\frac{1}{N/3}$ normalizes the energy as the Kac procedure.

A. Thermodynamic limit of a triangular antiferromagnet with long-range interactions

The free energy of model (2) is obtained by the Bragg-Williams approximation as follows. Let the sublattice

magnetizations be

$$m_{\rm A}=\frac{3}{N}\sum_{i\in{\rm A}}^{N/3}\sigma_i,\quad m_{\rm B}=\frac{3}{N}\sum_{i\in{\rm B}}^{N/3}\sigma_i,$$
$$\text{and}\quad m_{\rm C}=\frac{3}{N}\sum_{i\in{\rm C}}^{N/3}\sigma_i. \tag{3}$$

The energy for large N is given by

$$E_{\rm MF}=N\Big(-\frac{1}{6}J_1z(m_{\rm A}m_{\rm B}+m_{\rm B}m_{\rm C}+m_{\rm C}m_{\rm A})$$
$$-\frac{1}{6}J_2z\big(m_{\rm A}^2+m_{\rm B}^2+m_{\rm C}^2\big)\Big)$$
$$-h\frac{N}{3}(m_{\rm A}+m_{\rm B}+m_{\rm C}). \tag{4}$$

The entropy for size N is expressed as

$$S=k_B\ln W,$$
$$W=\frac{\frac{N}{3}!\frac{N}{3}!\frac{N}{3}!}{N_{\rm A}!\big(\frac{N}{3}-N_{\rm A}\big)!N_{\rm B}!\big(\frac{N}{3}-N_{\rm B}\big)!N_{\rm C}!\big(\frac{N}{3}-N_{\rm C}\big)!}, \tag{5}$$

where $N_{\rm A}$, $N_{\rm B}$, and $N_{\rm C}$ denote the number of up spins on sublattices A, B, and C, respectively. Thus, for large N, by making use of Stirling's formula, the entropy is given by

$$S_{\rm MF}=-\frac{N}{3}k_{\rm B}\Big(\frac{1+m_{\rm A}}{2}\ln\frac{1+m_{\rm A}}{2}+\frac{1-m_{\rm A}}{2}\ln\frac{1-m_{\rm A}}{2}$$
$$+\frac{1+m_{\rm B}}{2}\ln\frac{1+m_{\rm B}}{2}+\frac{1-m_{\rm B}}{2}\ln\frac{1-m_{\rm B}}{2}$$
$$+\frac{1+m_{\rm C}}{2}\ln\frac{1+m_{\rm C}}{2}+\frac{1-m_{\rm C}}{2}\ln\frac{1-m_{\rm C}}{2}\Big). \tag{6}$$

Then the free energy in the thermodynamic limit (MF free energy) is given by

$$F_{\rm MF}=E_{\rm MF}-TS_{\rm MF}. \tag{7}$$

This is also obtained using

$$S_{\rm MF}=-k_{\rm B}\sum_{\sigma_1,\ldots,\sigma_N}P(\sigma_1,\ldots,\sigma_N)\ln P(\sigma_1,\ldots,\sigma_N), \tag{8}$$

where

$$P(\sigma_1,\ldots,\sigma_N)=\prod_{i\in{\rm A}}P_1^{\rm A}(\sigma_i)\prod_{i\in{\rm B}}P_1^{\rm B}(\sigma_i)\prod_{i\in{\rm C}}P_1^{\rm C}(\sigma_i). \tag{9}$$

Here $P_1^{\rm A}(\pm1)=(1\pm m_{\rm A})/2$ is the single-site probability for state σ_i of sublattice A [$P_1^{\rm B}(\pm1)$ and $P_1^{\rm C}(\pm1)$ are defined in the same manner].

The self-consistent field (SCF) equations for the sublattice magnetizations are given by

$$\frac{\partial F_{\rm MF}}{\partial m_{\rm A}}=0,\quad \frac{\partial F_{\rm MF}}{\partial m_{\rm B}}=0,\quad\text{and}\quad \frac{\partial F_{\rm MF}}{\partial m_{\rm C}}=0, \tag{10}$$

which leads to

$$m_\mu=\tanh\Big(\frac{1}{2}\beta zJ_1(m_\nu+m_\lambda)+\beta zJ_2m_\mu+\beta h\Big), \tag{11}$$

where (μ,ν,λ) denote (A,B,C), (B,C,A), and (C,A,B), respectively. The solutions of Eq. (11) are given by $m_{\rm A}=m_{\rm B}=m_{\rm C}=0$ (D), $m_{\rm A}=-m_{\rm B}$ and $m_{\rm C}=0$ (PD), $m_{\rm A}\neq m_{\rm B}\neq m_{\rm C}$ and $m_{\rm A}\neq m_{\rm C}$ (3-FR), and $m_{\rm A}=m_{\rm B}\neq m_{\rm C}$ (2-FR) (the order of A, B, and C is arbitrary).

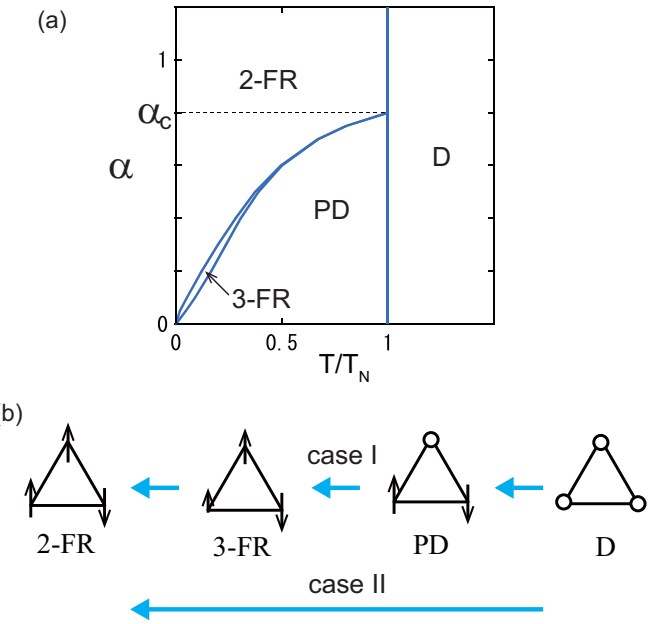

FIG. 2. (a) Phase diagram for α vs T. (b) Plaquette states of possible phases: two-sublattice ferrimagnetic (2-FR) state, three-sublattice ferrimagnetic (3-FR) state, partially disordered (PD) state, and disordered (D) state.

The highest critical temperature at which Z_6 symmetry is broken is $T_{\rm N}=zJ_2-zJ_1/2$. In case I ($\alpha<\alpha_{\rm C}$), the PD phase appears, while in case II ($\alpha>\alpha_{\rm C}$) the 2-FR phase appears, where

$$\alpha=2\frac{J_2}{|J_1|} \tag{12}$$

and the critical value is $\alpha_{\rm C}\simeq0.8$ [60]. The phase diagram for the ordered states is depicted in Figs. 2(a) and 2(b):

Case I. With decreasing temperature, the D phase, PD phase, 3-FR phase, and 2-FR phase appear successively.

Case II. Only one continuous transition occurs between the D and the 2-FR phases (Fig. 2).

The magnetization per site is defined as $m\equiv\frac{1}{3}(m_{\rm A}+m_{\rm B}+m_{\rm C})$ and the magnetic susceptibility per site is given by

$$\chi=\frac{dm}{dh}\Big|_{h=0}=\frac{3a_1^2+uv+vw+wu+2a_1(u+v+w)}{9\big(-2a_1^3-a_1^2(u+v+w)+uvw\big)}, \tag{13}$$

where $a_1=J_1z_1$, $u=\frac{1}{\beta}\cosh^2\beta J_1(\frac{z}{2}(m_{\rm B}+m_{\rm C})+\frac{\alpha}{2}zm_{\rm A})-J_2z$, $v=\frac{1}{\beta}\cosh^2\beta J_1(\frac{z}{2}(m_{\rm C}+m_{\rm A})+\frac{\alpha}{2}zm_{\rm B})-J_2z$, and $w=\frac{1}{\beta}\cosh^2\beta J_1(\frac{z}{2}(m_{\rm A}+m_{\rm B})+\frac{\alpha}{2}zm_{\rm C})-J_2z$.

We give in Fig. 3 typical temperature dependences of $m_{\rm A}$, $m_{\rm B}$, $m_{\rm C}$, and m at $\alpha=0.6$ and $\alpha=0.8\simeq\alpha_{\rm C}$. The magnetic susceptibilities χ are also shown. Here we set $J_1=-0.1$ and use the unit $k_B=1$, which is also applied hereafter. We found that for $\alpha>0.8$ qualitatively the same features of χ, $m_{\rm A}$, $m_{\rm B}$, and $m_{\rm C}$ as for $\alpha=0.8$ are realized, and the case $\alpha=0.8$ is regarded as case II.

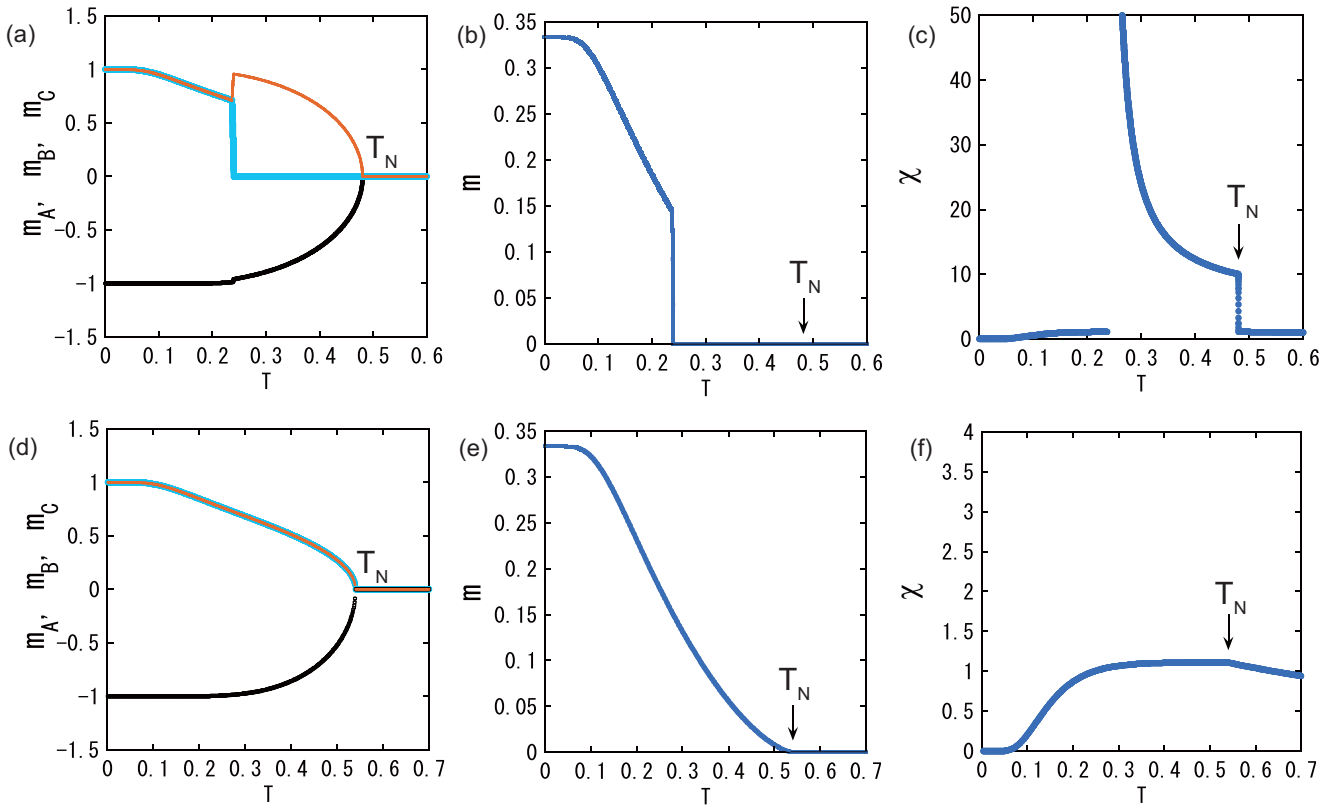

FIG. 3. Properties of the LRTIAFF model in the thermodynamic limit (MF theory). For $\alpha = 0.6$, temperature dependences of (a) sublattice magnetizations ($m_{\rm A}$, $m_{\rm B}$, and $m_{\rm C}$), (b) magnetization (m), and (c) susceptibility χ. For $\alpha = 0.8$, (d) sublattice magnetizations, (e) magnetization, and (f) susceptibility. For $\alpha = 0.6$ and 0.8, $T_{\rm N} = 0.48$ and 0.54, respectively.

It should be noted that there is a prominent difference between the two cases. The susceptibility diverges in the former, while it does not in the latter. A magnified detail of m and χ around the 3-FR phase for $\alpha = 0.6$ is depicted in Fig. 4. The susceptibility diverges at $T_{\rm c2}$ between the PD and the 3-FR phases and shows a finite jump at $T_{\rm c1}$ between the 3-FR and the 2-FR phases. A jump of the susceptibility at $T_{\rm c1}$ has not been seen so far.

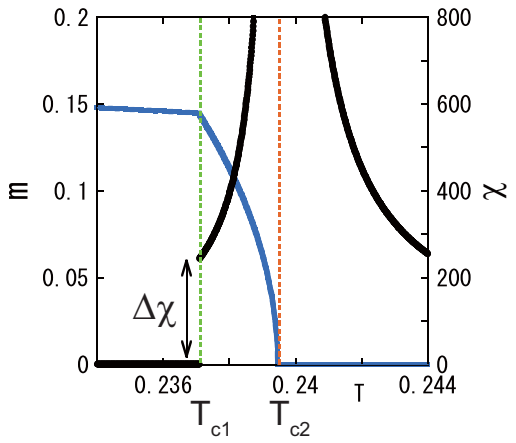

FIG. 4. Magnified detail of m (blue line) and χ (black line) around the 3-FR region for $\alpha = 0.6$, in which $T_{\rm c1} \simeq 0.2371$ is the transition point between the 2-FR and the 3-FR phases, and $T_{\rm c2} \simeq 0.2395$ is that between the 3-FR and the PD phases. χ diverges at $T_{\rm c2}$ and shows a finite jump at $T_{\rm c1}$.

In the latter case, although the 2-FR phase has nonzero magnetization at low temperatures, the magnetization of the 2-FR is 0 at the transition point, at which the sublattice magnetizations are given as $(m_{\rm A}, -m_{\rm A}/2, -m_{\rm A}/2)$. The sublattice magnetization appears as $m_{\rm A} \sim \sqrt{t}$ around $T_{\rm N}$, where $t \equiv \frac{T_{\rm N}-T}{T_{\rm N}}$, while the critical amplitude of $\sqrt{t}$ (the leading term) for uniform magnetization ($m = m_{\rm A} + m_{\rm B} + m_{\rm C}$) becomes 0. This suppression of magnetization growth causes nondivergence of the magnetic susceptibility χ.

B. Finite-size effects of a triangular antiferromagnet with long-range interactions

1. Method

We investigate finite-size effects of model (2) on the phase transition. For this purpose, we apply importance-sampling Metropolis Monte Carlo simulations. In order to characterize the phase, we introduce the following three order parameters.

First, we define the mean-square value of magnetization as

$$m^2 = \frac{1}{N^2}\left\langle \left(\sum_i^N \sigma_i \right)^2 \right\rangle, \tag{14}$$

where $\langle\,\rangle$ denotes the thermal average.

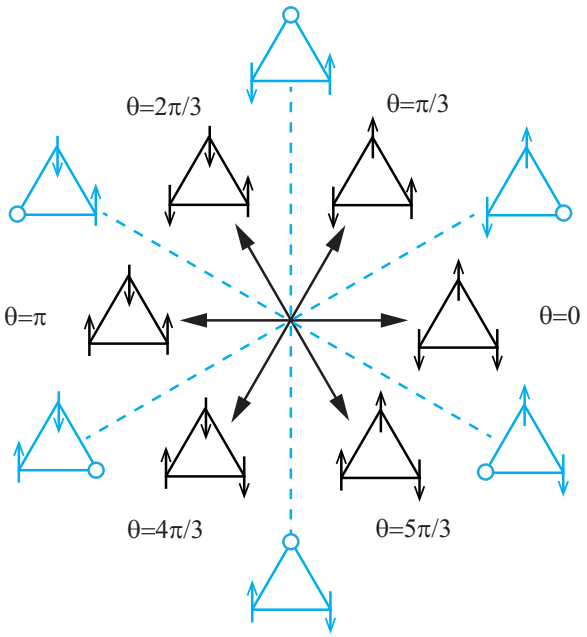

FIG. 5. Six plaquette states of the ferrimagnetic state. Six angles, $\theta = 0, \frac{\pi}{3}, \frac{2\pi}{3}, \pi, \frac{4\pi}{3}$, and $\frac{5\pi}{3}$, are allocated for the plaquette states. Six plaquette states for the PD phase are given in the directions of the dotted lines.

Second, we define the order parameter to detect the breaking of Z_6 symmetry,

$$M^2 = \frac{1}{N_p^2}\left\langle\left[\left\{\sum_{m=1}^{N_p}\cos\theta_m\right\}^2 + \left\{\sum_{m=1}^{N_p}\sin\theta_m\right\}^2\right]\right\rangle, \quad (15)$$

where

$$\vec{M} = (M_x, M_y) = \left(\frac{1}{N_p}\sum_{m=1}^{N_p}\cos\theta_m,\ \frac{1}{N_p}\sum_{m=1}^{N_p}\sin\theta_m\right). \quad (16)$$

Here θ_m is the angle of the vector allocated for plaquette m and is given by $\theta_m = \frac{2\pi}{6}k$, where k takes $k = 0, 1, \ldots 5$ (Fig. 5). N_p is the number of triangular plaquettes, i.e., $N_p = N/3$.

Third, to identify the PD phase, we define the following order parameter:

$$\mathcal{M}_6 = \langle \mathrm{Re}[(M_x + iM_y)^6]\rangle. \quad (17)$$

The PD phase is a mixed phase of two 2-FR phases and the difference in the angles of the 2-FR phases in the six-clock modes (Fig. 5) is $\pi/3$.

If the PD phase is realized, $\mathcal{M}_6$ should be negative, $\mathcal{M}_6 < 0$, while if the 2-FR phase is realized, $\mathcal{M}_6$ should be positive. Thus we can distinguish the two orders. In later discussion we compare the behavior between $M^6 = (M^2)^3$ and $\mathcal{M}_6$ at the same power.

Magnetic susceptibility is defined as

$$\chi = \frac{1}{NT}\left[\left\langle\left(\sum_i^N \sigma_i\right)^2\right\rangle - \left\langle\sum_i^N \sigma_i\right\rangle^2\right]. \quad (18)$$

2. *Results*

We plot in Figs. 6(a) and 6(b) the temperature dependences of m^2 and χ, respectively, for $\alpha = 0.6$ (case I) for several system sizes: $N = L \times L$, where L is the linear dimension of the system. The temperature dependences of $M^6 \equiv (M^2)^3$ and $\mathcal{M}_6$ are also shown in Fig. 6(c).

In the period $0.24 \lesssim T \leqslant T_N$, $m^2 = 0$ and $\mathcal{M}_6 < 0$ and thus the phase of this region is identified as PD. Then we find the 3-FR region, where m^2 increases rapidly from 0, and also a divergence of χ around $T = 0.24$, which is identified as the transition point between the PD and the 3-FR phases estimated in the MF theory. These indicate that the properties of finite-size systems in case I can be expected from the MF results shown in Figs. 3 and 4.

Next we show the temperature dependences of m^2 and χ for $\alpha = 0.8$ (case II close to the critical case) and $\alpha = 0.9$ (case II) in Fig 7. As shown in Fig. 3, for $\alpha > \alpha_C$ the MF analysis shows no divergence of the magnetic susceptibility at the transition point between the 2-FR and the D phases. There, χ is a continuous function of T and the transition point is given at $T_N = 0.54$ and $T_N = 0.57$ for $\alpha = 0.8$ and $\alpha = 0.9$, respectively. However, as shown in Fig. 7, χ shows divergencelike behavior around $T = 0.45$ for $\alpha = 0.8$ and $T = 0.50$ for $\alpha = 0.9$.

Although the LRTIAFF model is expected to show the properties obtained in the MF analysis, we found a peculiar

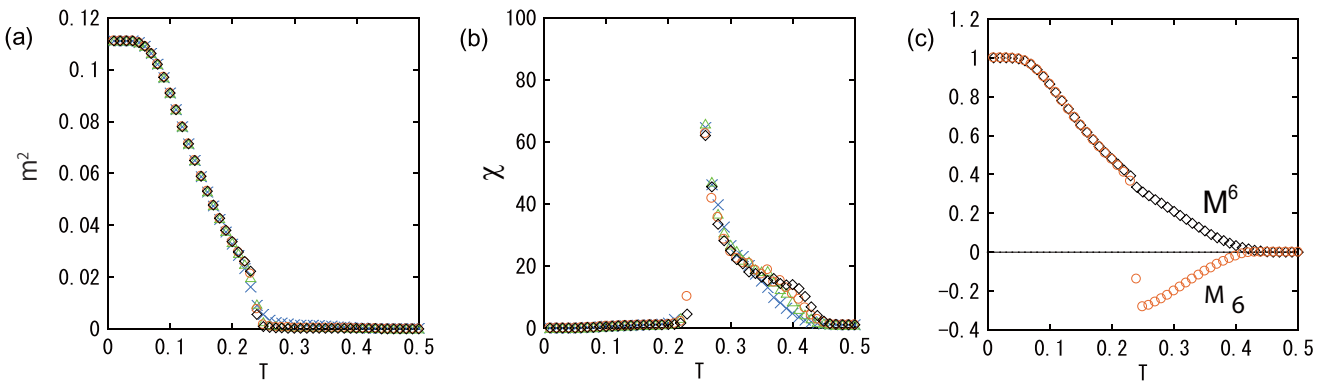

FIG. 6. MC profiles for $\alpha = 0.6$. Temperature dependences of (a) m^2 and (b) χ for different system sizes. Crosses denote $L = 72$; triangles, $L = 108$; circles, $L = 144$; and diamonds, $L = 192$. (c) Temperature dependences of M^6 (black diamonds) and $\mathcal{M}_6$ (red circles) for $L = 192$.

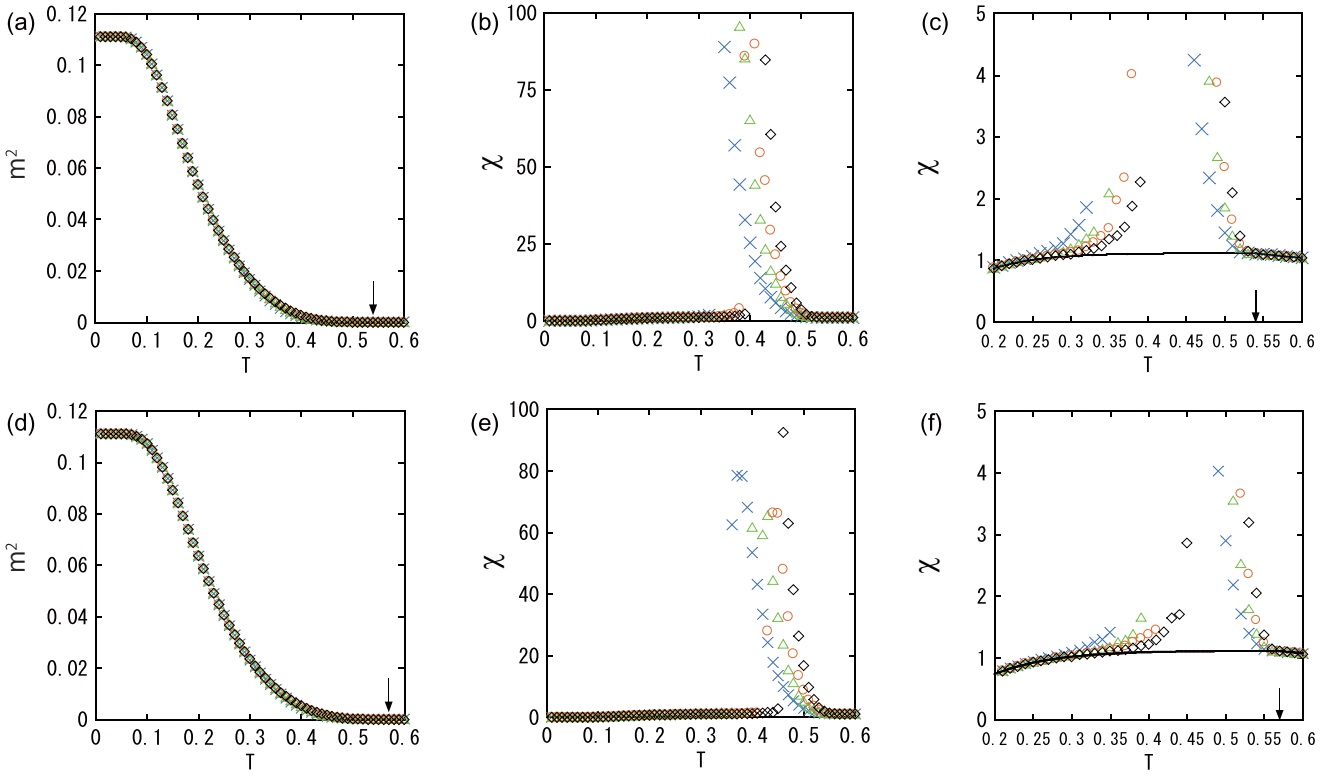

FIG. 7. For $\alpha = 0.8$, temperature dependences of (a) m^2 and (b) χ and (c) magnified view around the divergencelike enhancement region of χ for different system sizes. Crosses denote $L = 72$; triangles, $L = 10$; circles, $L = 144$; and diamonds, $L = 192$. Comparison of χ between the thermodynamic limit (i.e., the MF result; solid line) and finite-size systems is given in (c). For $\alpha = 0.9$, temperature dependences of (d) m^2 and (e) χ and (f) magnified view around the divergencelike enhancement region of χ with a comparison with the MF result (solid line). Arrows denote the critical temperatures $T_N = 0.54$ and 0.57 for $\alpha = 0.8$ and $\alpha = 0.9$, respectively, in the thermodynamic limit (the MF theory).

difference between the MF analysis and the MC method. Because the LRTIAFF model should give the MF properties in the thermodynamic limit, the difference should be attributed to the finite-size effect. Comparisons are shown in Figs. 7(c) and 7(f).

To find the origin of this contradiction, we study the temperature dependences of $M^6 \equiv (M^2)^3$ and $\mathcal{M}_6$ for case II ($\alpha = 0.8$ and $\alpha = 0.9$) (see Fig. 8). We may expect that $\mathcal{M}_6$ and M^6 will appear simultaneously around $T_N = 0.54$ and 0.57 for $\alpha = 0.8$ and 0.9, respectively, and show a monotonic increase below these temperatures. In Fig. 8, however, in both cases we find that while M^6 appears around the expected temperature, $\mathcal{M}_6$ appears at a much lower temperature. That is, it seems that $\mathcal{M}_6 = 0$ in the range $0.45 \lesssim T \leqslant T_N$ for $\alpha = 0.8$ and in the range $0.5 \lesssim T \leqslant T_N$ for $\alpha = 0.9$.

With decreasing temperature, the breaking of Z_6 symmetry takes place at T_N, where M^6 appears, but no specific order in the representation of the 6SC mode appears, i.e., $\mathcal{M}_6 = 0$, over a range of temperatures. This may indicate the existence of a kind of masslesslike region in the notation of the 6SC state. Because the sublattice magnetization is already developed ($M^6 > 0$), we consider that in this range of temperatures, both the 2-FR order and the PD order appear. Then, the contribution of the 2-FR order (i.e., $\mathcal{M}_6 > 0$) and that of the PD order ($\mathcal{M}_6 < 0$) cancel each other, and as a result $\mathcal{M}_6 = 0$ is realized.

Here we study the cause of the divergencelike enhancement of χ for case II connecting the disappearance of $\mathcal{M}_6$. In the

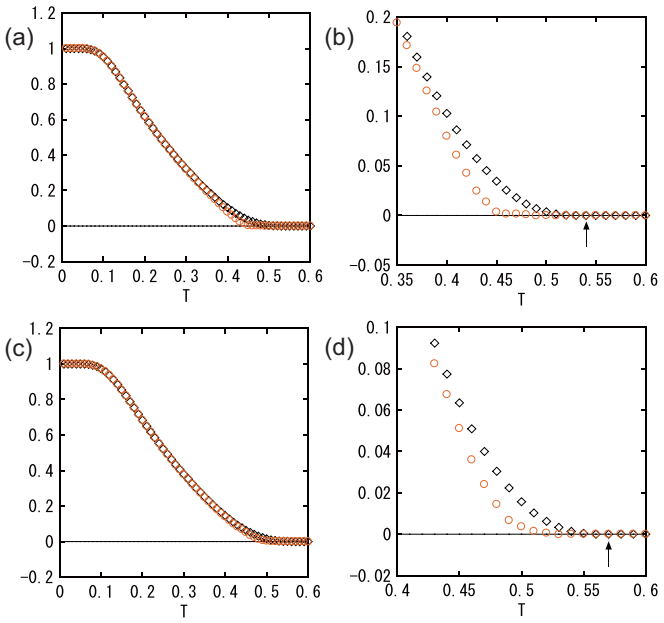

FIG. 8. Temperature dependences of M^6 (black diamonds) and $\mathcal{M}_6$ (red circles) for (a) $\alpha = 0.8$ and (c) $\alpha = 0.9$. The system size is $L = 192$. Magnified views of M^6 and $\mathcal{M}_6$ around T_N for (a) and (c) are given in (b) and (d), respectively. Arrows denote the critical temperatures $T_N = 0.54$ and 0.57 for $\alpha = 0.8$ and $\alpha = 0.9$, respectively, in the thermodynamic limit (the MF theory).

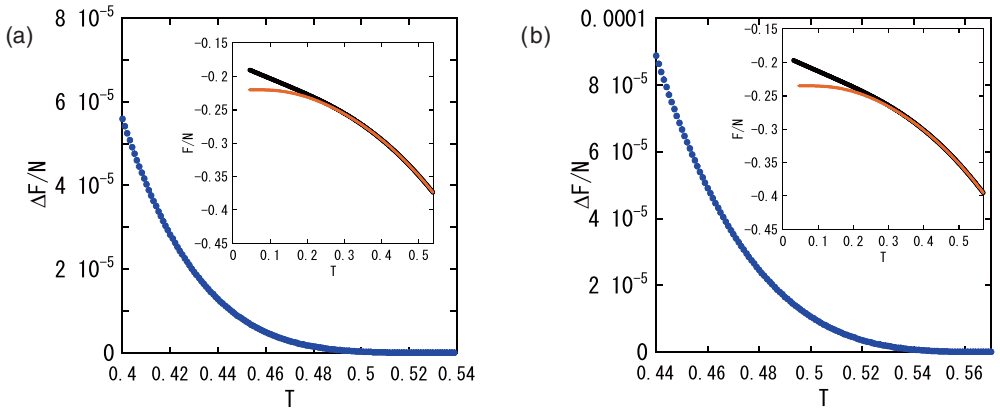

FIG. 9. Temperature dependence of $\Delta F/N$ for (a) $\alpha = 0.8$ and (b) $\alpha = 0.9$. Insets: Temperature dependence of F/N for 2-FR (thin red lines) and PD (thick black lines) phases.

MF analysis for case II, the 2-FR phase appears and the free energy of the 2-FR phase is lower than that of the PD phase. The susceptibility was calculated at the minimum point of the free energy, which is finite as shown in Fig. 3. However, the observation using the MC method indicates that the emergence probabilities of the 2-PR and PD phases are close, i.e., the free energies of the phases are close.

In Fig. 9, we plot the difference in the MF free energies between the PD and the 2-FR phases for the cases of both $\alpha = 0.8$ and $\alpha = 0.9$,

$$\Delta F/N \equiv \frac{1}{N}(F_{\rm PD} - F_{\text{2-FR}}), \tag{19}$$

where N $(=L^2)$ is the system size. ΔF values are monotonic decreasing functions of T. It should be noted that the difference is 0 at $T_{\rm N}$ because the modes $(m_{\rm A}, -m_{\rm A}, 0)$ and $(m_{\rm A}, -m_{\rm A}/2, -m_{\rm A}/2)$ degenerate.

For $\alpha = 0.8$, the difference in susceptibility between the MF and the MC results [Fig. 7(c)] was found around $T = 0.45$ for $L = 192$. $\Delta F/N$ at around $T = 0.45$ is about 10^{-5}, and for a system of $L = 2 \times 10^2$ and $N = 4 \times 10^4$,

$$\Delta F = \Delta F/N \times N \simeq 4 \times 10^{-1}, \tag{20}$$

which is about the order of the temperature. Thus, the probability of the PD phase is not negligible for this system size, although it becomes 0 in the thermodynamic limit $(N \to \infty)$. In the period $0.45 \lesssim T \leqslant T_{\rm N}$, due to this quasidegeneracy, the two phases contribute, and a masslesslike situation is realized.

It is expected that for larger α in case II, the stability of the 2-FR phase around $T_{\rm N}$ is stronger and $\Delta F/N$ becomes larger. Indeed this tendency is shown in Fig. 9, but even for $\alpha = 0.9$, $\Delta F/N$ is small enough to cause the quasidegeneracy and the same consideration holds, i.e., the degenerate region is $0.5 \lesssim T \leqslant T_{\rm N}$, which gives $\Delta F/N \lesssim 10^{-5}$.

Upon lowering the temperature the difference in the free energy $\Delta F/N$ becomes larger. When the difference is the same order as the temperature, the degenerate states are resolved and the 2-FR state becomes dominant.

As for the divergence of χ we propose the following picture. In the degenerate region, we define $p_{\rm FR}$ $(p_{\rm PD})$ as the probability of realizing the 2-FR (PD) phase in the MC simulation, where $p_{\rm FR} + p_{\rm PD} = 1$, and the magnetization for the 2-FR (PD) phase is given by $m_{\rm FR} \equiv \langle \sum_i^N \sigma_i \rangle_{\rm FR}$ $(m_{\rm PD} \equiv \langle \sum_i^N \sigma_i \rangle_{\rm PD})$.

We have the following estimation up to the order of N^2. Because $m_{\rm PD} = 0$,

$$\left\langle \left(\sum_i^N \sigma_i \right)^2 \right\rangle \sim p_{\rm FR} N^2 m_{\rm FR}^2 + O(N) \tag{21}$$

and

$$\left\langle \sum_i^N \sigma_i \right\rangle^2 = (p_{\rm FR} N m_{\rm FR})^2. \tag{22}$$

Thus we have

$$\chi = \frac{1}{N} \frac{\left\langle \left(\sum_i^N \sigma_i \right)^2 \right\rangle - \left\langle \sum_i^N \sigma_i \right\rangle^2}{T} \sim N \frac{m_{\rm FR}^2 (p_{\rm FR} - p_{\rm FR}^2)}{T} + O(1). \tag{23}$$

Before the temperature approaches the energy gap $\sim 10^{-5}$ in cooling, $m_{\rm FR} \simeq 0$ and thus $\chi = O(1)$. When the 2-FR phase is dominant in the cases $\alpha = 0.8$ and 0.9 (case II), i.e., $m_{\rm FR} \neq 0$ and $1/2 < p_{\rm FR} < 1$, we expect $\chi \sim O(N)$, which explains the observation of MC simulation. Namely a divergencelike enhancement of χ is observed at temperatures with the same order as the energy gap. At lower temperatures, the state is in the FR phase and $p_{\rm FR} \simeq 1$ and χ will be $O(1)$ again.

Thus we conclude that the LRTIAFF model has a peculiar free energy structure in which the 2-FR and PD phases are nearly degenerate in the vicinity of $T_{\rm N}$, which causes a divergencelike enhancement of the magnetic susceptibility χ by a finite-size effect but it is robust even at large sizes, i.e., $L \simeq O(10^2)$.

III. GENERALIZED SIX-STATE CLOCK MODEL WITH LONG-RANGE INTERACTIONS

In this section we study a more general model with Z_6 symmetry with a set of six states:

$$S_i = 0, 1, \ldots 5. \tag{24}$$

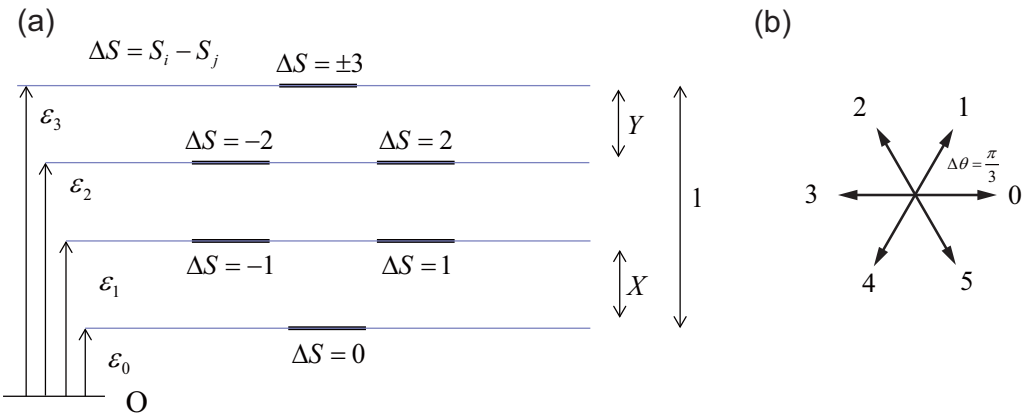

FIG. 10. (a) Energy diagram of the generalized six-state clock model. (b) Six clock modes (vectors) of the generalized six-state clock model. The angle $\theta = \frac{2\pi S}{6}$ is allocated for each state $S = 0, \ldots, 5$.

The Hamiltonian of the symmetric Z_6 model (i.e., not chiral) is given by the following general form [Fig. 10(a)]:

$$\mathcal{H}_{\mathrm{G6}} = \sum_{\langle i,j\rangle} (\epsilon_0 \delta_{S_i,S_j} + \epsilon_1 \delta_{S_i,S_j\pm 1} + \epsilon_2 \delta_{S_i,S_j\pm 2} + \epsilon_3 \delta_{S_i,S_j\pm 3}), \tag{25}$$

where δ_{S_i,S_j} is defined as $\delta = 1$ if $S_i = S_j \pmod 6$ and 0 otherwise. The model can be expressed by the generalized six-state clock model,

$$\mathcal{H}'_{\mathrm{G6}} = \sum_{\langle i,j\rangle} (-J_0 - J_1 \cos(\theta_i - \theta_j) - J_2 \cos^2(\theta_i - \theta_j) - J_3 \cos^3(\theta_i - \theta_j)), \tag{26}$$

where θ_i denotes the angle of the clock models [Fig. 10(b)]:

$$\theta_i = \frac{2\pi S_i}{6}. \tag{27}$$

These two models are converted to each other by the linear transformation

$$\begin{pmatrix} \epsilon_0 \\ \epsilon_1 \\ \epsilon_2 \\ \epsilon_3 \end{pmatrix} = \begin{pmatrix} -1 & -1 & -1 & -1 \\ -1 & -1/2 & -1/4 & -1/8 \\ -1 & 1/2 & -1/4 & 1/8 \\ -1 & 1 & -1 & 1 \end{pmatrix} \begin{pmatrix} J_0 \\ J_1 \\ J_2 \\ J_3 \end{pmatrix}. \tag{28}$$

We define

$$X = \frac{\epsilon_1 - \epsilon_0}{\epsilon_3 - \epsilon_0} \quad \text{and} \quad Y = \frac{\epsilon_3 - \epsilon_2}{\epsilon_3 - \epsilon_0} \tag{29}$$

[Fig. 10(a)] as essential parameters to identify the pattern of phase transitions (see the following sections). When $X = Y = 1/4$ for Eq. (25) or $J_1 \neq 0$ and $J_2 = J_3 = 0$ for Eq. (26), it corresponds to the six-state clock model.

Hereafter we study the long-range interacting model for Eq. (25) or, equivalently, for Eq. (26), in which the sum runs over all the pairs ($\langle ij\rangle$ is replaced by $i < j$) and the parameters are normalized by N, i.e., $\epsilon_i \to \frac{\epsilon_i}{N} \ldots$ and $J_i \to \frac{J_i}{N} \ldots$ ($i = 0$, 1, 2, and 3). We call these two equivalent expressions the *long-range generalized six-state clock* (LRG6SC) model.

A. Thermodynamic limit of the long-range generalized six-state clock model

In this subsection we build SCF equations for the LRG6SC model in the thermodynamic limit. The SCF equations for model (25) are derived as follows. For this purpose, we apply the idea of the Bragg-Williams approximation to the model. The MF energy for model (25) is given by

$$E_{\mathrm{G6,MF}} = \frac{1}{2} N z \sum_{i=0}^{5} \sum_{j=0}^{5} E_{S_i,S_j} P(S_i) P(S_j), \tag{30}$$

where E_{S_i,S_j} is the energy between site i and site j, i.e.,

$$E_{S_i,S_j} = \epsilon_0 \delta_{S_i,S_j} + \epsilon_1 \delta_{S_i,S_j\pm 1} + \epsilon_2 \delta_{S_i,S_j\pm 2} + \epsilon_3 \delta_{S_i,S_j\pm 3}, \tag{31}$$

and $P(S_i)$ is the probability for state S_i. The entropy of the system is

$$S_{\mathrm{MF}} = -N k_B \sum_{S_i=0}^{5} P(S_i) \ln P(S_i). \tag{32}$$

Thus the MF free energy is given by

$$F_{\mathrm{G6,MF}} = E_{\mathrm{G6,MF}} - T S_{\mathrm{MF}}. \tag{33}$$

We derive SCF equations under the condition that $\sum_{S_i=0}^{5} P(S_i) = 1$. With the method of the Lagrange multiplier, we minimize the following quantity:

$$f \equiv F_{\mathrm{G6,MF}} - \lambda \left(\sum_{S_i=0}^{5} P(S_i) - 1 \right). \tag{34}$$

The condition for the extreme value on $P(S_i)$ ($S_i = 0, \ldots, 5$) is given by $\frac{\partial f}{\partial P(S_i)} = 0$ for $S_i = 0, \ldots, 5$ and $\frac{\partial f}{\partial \lambda} = 0$.

Eliminating λ dependence in the equations, we have five SCF equations and one condition,

$$z \left(\sum_{k=0,1,\ldots,5} E_{l,k} P(k) - \sum_{k=0,1,\ldots,5} E_{0,k} P(k) \right) + k_B T (\ln P(l) - \ln P(0)) = 0 \tag{35}$$

for $l = 1, 2, 3, 4$, and 5, and

$$\sum_{k=0}^{5} P(k) = 1. \tag{36}$$

Here let us relate the LRTIAFF model, (2), and the LRG6SC model, (25) [or (26)]. As shown in Fig. 1, the plaquette state with three spins (σ^{A}, σ^{B}, σ^{C}) in the LRTIAFF model corresponds to an angle $\theta(=\frac{2\pi S}{6})$ (S takes 0, ..., or 5) at the superlattice denoted by shaded triangles in Fig. 1. In the present paper, we restrict $X = Y$, which is regarded as a natural extension of the LRTIAFF model, (2), from the following consideration. Let the ground state (GS) of model (2) be the complete 2-FR state with state (σ^{A},σ^{B},σ^{C}) = ($\downarrow$, $\downarrow$, $\uparrow$), i.e., $\theta = 0$ as depicted in Fig. 1.

If one plaquette state changes to ($\downarrow$, $\uparrow$, $\uparrow$), i.e., $\theta = \pi/3$, the energy of the NN interactions (J_1) does not change because of the degeneracy due to the frustration. However, the energy of the NNN interactions (J_2) increases by

$$E_1 - E_0 = \frac{J_2}{N/3} \times \left(\frac{N}{3} - 1\right) \times 2 \simeq 2J_2, \tag{37}$$

where E_0 is the GS energy and E_1 is the energy for $\theta = \pi/3$. If the plaquette state further changes to the state $\theta = 2\pi/3$, i.e., ($\downarrow$, $\uparrow$, $\downarrow$), the excitation energy from the GS is

$$\begin{aligned} E_2 - E_0 &= \frac{J_2}{N/3} \times \left(\frac{N}{3} - 1\right) \times 4 + \frac{|J_1|}{N/3} \times \left(\frac{2N}{3} - 2\right) \times 2 \\ &\simeq 2(2|J_1| + 2J_2). \end{aligned} \tag{38}$$

The excitation energy for state $\theta = \pi$ ($\uparrow$, $\uparrow$, $\downarrow$) is

$$\begin{aligned} E_3 - E_0 &= \frac{J_2}{N/3} \times \left(\frac{N}{3} - 1\right) \times 6 + \frac{|J_1|}{N/3} \times \left(\frac{2N}{3} - 2\right) \times 2 \\ &\simeq 2(2|J_1| + 3J_2). \end{aligned} \tag{39}$$

We find $E_1 - E_0 = E_3 - E_2$, and thus we have $\epsilon_1 - \epsilon_0 = \epsilon_3 - \epsilon_2$. That is, $X = Y$ for the LRG6SC model.

Now we study the ordering process of the model. Equations (35) and (36) are solved numerically by the Newton-Raphson method. The phases which appear in the LRTIAFF model can be classified into the following solutions of the LRG6SC model.

(a) The 2-FR phase is given at $P(0) < P(1) = P(5) < P(2) = P(4) < P(3)$.

(b) The 3-FR phase is given at $P(0) < P(1) < P(5) < P(2) < P(4) < P(3)$ or $P(0) < P(5) < P(1) < P(4) < P(2) < P(3)$.

(c) The PD phase is given at $P(0) = P(1) < P(2) = P(5) < P(3) = P(4)$.

(d) The D phase is given at $P(0) = P(1) = P(2) = P(3) = P(4) = P(5)$.

The cyclic permutation of $\{P(i)\}$ for these relations causes the same classification.

We define the order parameters to characterize the ordered state,

$$\tilde{m} = P(0) + P(2) + P(4) - P(1) - P(3) - P(5), \tag{40}$$

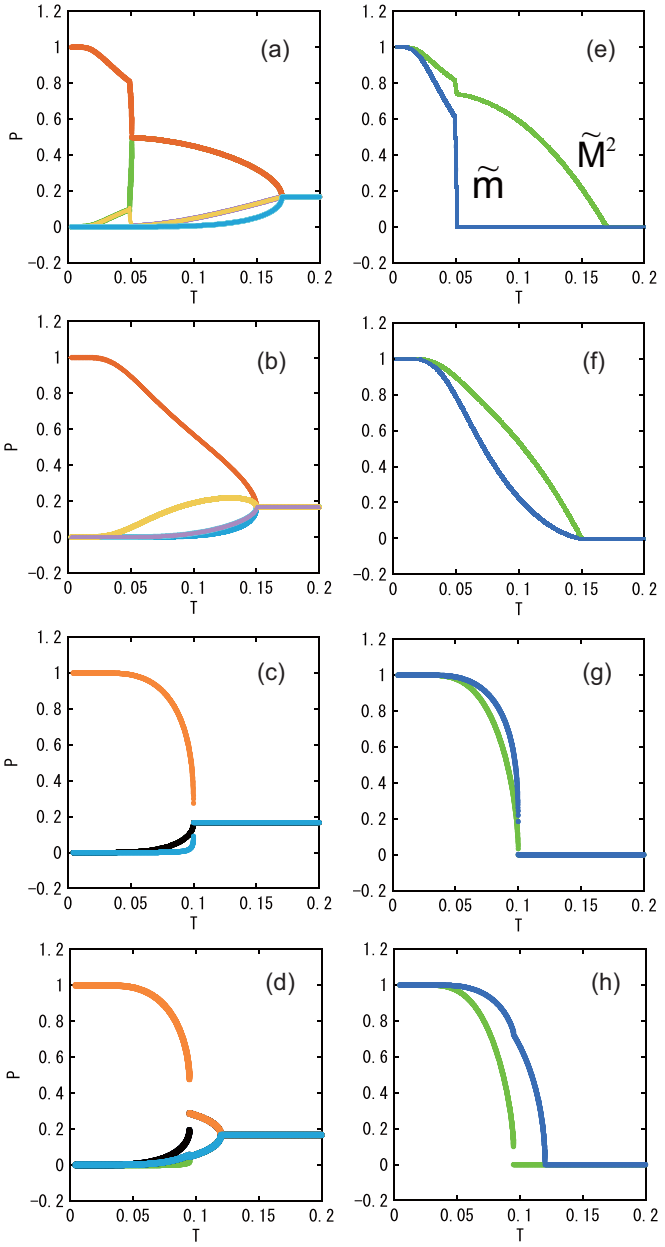

FIG. 11. Typical MF solutions $P(0), \ldots, P(5)$ for the generalized six-state clock model for (a) $X = 0.15$, (b) $X = 0.25$, (c) $X = 0.5$, and (d) $X = 0.55$ and corresponding $\tilde{m}$ (blue line) and $\tilde{M}^2$ (green line) for (e) $X = 0.15$, (f) $X = 0.25$, (g) $X = 0.5$, and (h) $X = 0.55$.

which is regarded as "magnetization" in the analogy between S_i [Fig. 10(b)] in the LRG6SC model and the plaquette state (Fig. 5) in the LRTIAFF model.

To study the breaking of Z_6 symmetry, we also define

$$\vec{\tilde{M}} = \sum_{q=0,\ldots,5} p(q)\vec{v}_q, \tag{41}$$

where $\vec{v}_q$ is a unit vector for the arrow in Fig. 9(b). The susceptibility is defined as $\tilde{\chi} = \frac{d\tilde{m}}{dh}|_{h=0}$, where the MF energy under a field is given by $E_{\mathrm{G6,MF}} - h\tilde{m}$.

In Fig. 11, we show the temperature dependences of typical solutions $P(i)$ and ordering processes $\tilde{m}$ and $\tilde{M}^2$ for various

values of X. They are classified into four kinds of transition patterns in the period $0 < X < 1$. The region $0 < X < 0.5$ for the LRG6SC model corresponds to $0 < \alpha$ for the LRTIAFF model, and α_C corresponds to $X_C = 0.2$ (Appendix B).

For $X = 0.15 < X_C$, phase transitions successively occur from the D phase to the PD phase, to the 3-FR phase, and then to the 2-FR phase as shown in Figs. 11(a) and 11(e). This region corresponds to case I. For $X = 0.25 > X_C$, the D phase directly changes to the 2-FR phase as shown in Figs. 11(b) and 11(f). This region corresponds to case II. We found qualitatively the same nature as the finite-size effect discussed for the LRTIAFF model. The details are given in Appendix A.

At $X = 0.5$, discontinuous transitions for $\tilde{m}$ and $\tilde{M}$ occur at the same transition point. Here $\epsilon_1 = \epsilon_2$, and thus the energy structure [Fig. 10(a)] shows one stable, four degenerate, and one highest energy states. This degeneracy causes the system to be an effective five-state Potts model. The q-state Potts model with $q \geqslant 3$ shows a first-order phase transition in the dimension $d \geqslant 3$, and it holds in the MF model, and we found that the present model with $X = 0.5$ shows a first-order transition [61] [Figs. 11(c) and 11(g)]. Here the ordered state corresponds to the solution

$$P(0) < P(1) = P(2) = P(4) = P(5) < P(3).$$

For larger values of X, e.g., $X = 0.55$, we find that the transition point (call edT_2) of $\tilde{m}$ is higher than that (T_1) of $\tilde{M}$ [Figs. 11(d) and 11(h)], where

$$P(0) = P(2) = P(4) < P(1) = P(3) = P(5)$$

for $T_1 < T < T_2$, and

$$P(0) < P(2) = P(4) < P(1) = P(5) < P(3)$$

for $T < T_1$. The cyclic permutation of $\{P(i)\}$ for these relations causes the same classification.

Here, we may characterize the successive phase transitions by the following picture: with decreasing temperature the Z_2 symmetry of $\tilde{m}$ is broken first and then the breaking of Z_3 symmetry follows. The former process gives a second-order phase transition as the Ising model in the MF theory and the latter process causes a first-order phase transition as the three-state Potts model in the MF theory.

IV. DISCUSSION AND SUMMARY

We studied the finite-size effect of the long-range interaction model of the triangular Ising antiferromagnet with next-nearest-neighbor ferromagnetic interaction (LRTIAFF model). In the MF analysis corresponding to the thermodynamic limit, the susceptibility is a continuous function and does not show divergence at all temperatures for $\alpha > \alpha_C$. In contrast, we found a divergencelike enhancement of the susceptibility for $\alpha > \alpha_C$ around the transition point between the D and the 2-FR phases in the MC simulation of finite-size systems. We investigated the origin of this divergencelike behavior in the MC study and found that it is due to a peculiar degeneracy of the free energies of the PD and 2-FR phases. This degeneracy is not resolved in rather large systems [$L \sim O(10^2)$]. There, because of the small difference in the free energies, the probability of the PD phase is not negligible and the configuration migrates between the 2-FR and the PD phases. The former has a finite magnetization, while the latter has zero. With decreasing temperature, when the 2-FR phase becomes dominant, the susceptibility can be $O(N)$, which gives a divergencelike enhancement of the magnetic susceptibility. There the 2-FR phase appears as a sudden change, which looks like a first-order phase transition.

We also explored a general model of the cyclic Z_6 symmetry, which is expressed by the generalized six-state clock model, Eq. (25). We studied the phase transitions of the long-range generalized six-state clock (LRG6SC) model. The LRG6SC model covers a wider region of the models of Z_6 symmetry and phenomena similar to the LRTIAFF model are observed in part of the phase diagram. That is, for $0 < X < X_c = 0.20$, the 2-FR, 3-FR, PD, and D phases appear, which corresponds to case I for the LRTIAFF model, and for $X_c < X < 0.5$, the transition between the 2-FR and the D phases takes place, which corresponds to case II for the LRTIAFF model. The characteristics of the finite-size effect in the LRTIAFF model were also found in the LRG6SC model.

At $X = 0.5$, a Potts-type first-order transition occurs, in which both $\tilde{m}$ and $\tilde{M}$ show discontinuous jumps at the same temperature, and for $0.5 < X < 1$, the breaking Z_3 symmetry follows that of Z_2, which causes a first-order transition for $\tilde{m}$ and $\tilde{M}$ at a lower temperature and a second-order transition for $\tilde{m}$ at a higher temperature.

The phase transitions of the layered TIAFF model have been explained from the viewpoint of the RG of the 6SC model [62] making use of the Hamiltonian

$$\mathcal{H} = -J \sum_{\langle ij \rangle} \cos(\theta_i - \theta_j) - \lambda_6 \sum_i \cos(6\theta_i), \qquad (42)$$

where $0 \leqslant \theta_i < 2\pi$. Here the positive λ_6 gives sixfold anisotropy for $\theta_i = 2\pi k/6$, $k = 0, 1, \ldots 5$, which corresponds to the 2-FR state. It has been pointed out that the three-dimensional 6SC model exhibits behavior similar to that of the 3DXY model at relatively high temperatures but it is relevant over the whole low-temperature phase below the critical point of the 3DXY universality [62].

This situation was explained by a renormalization-group picture [25]. Along the coarse-graining process, λ_6 first decreases, which suggests that the system behaves as the 3DXY model, but it increases for larger scales, which means that the system is in an ordered phase with sixfold anisotropy. This dangerously irrelevant nature [63,64] is characteristic.

Similar RG flow diagrams were proposed for the layered TIAFF model without [21] and with [24] the NNN interaction, where the successive phase transitions (D $\rightarrow$ PD $\rightarrow$ 2-FR) have been explained by the change in the sign of λ_6. This picture holds in the 3D6SC model and the layered TIAFF model, which are short-range interaction models. In the present paper, however, long-range interaction models were studied and some difference may exist. The situation of nearly degenerate PD and 2-FR states around the critical point T_N is similar to that around the 3DXY fixed point in short-range interaction models, but the RG flows around T_N for long-range interaction models may be different from those around the 3DXY fixed point for short-range interaction models.

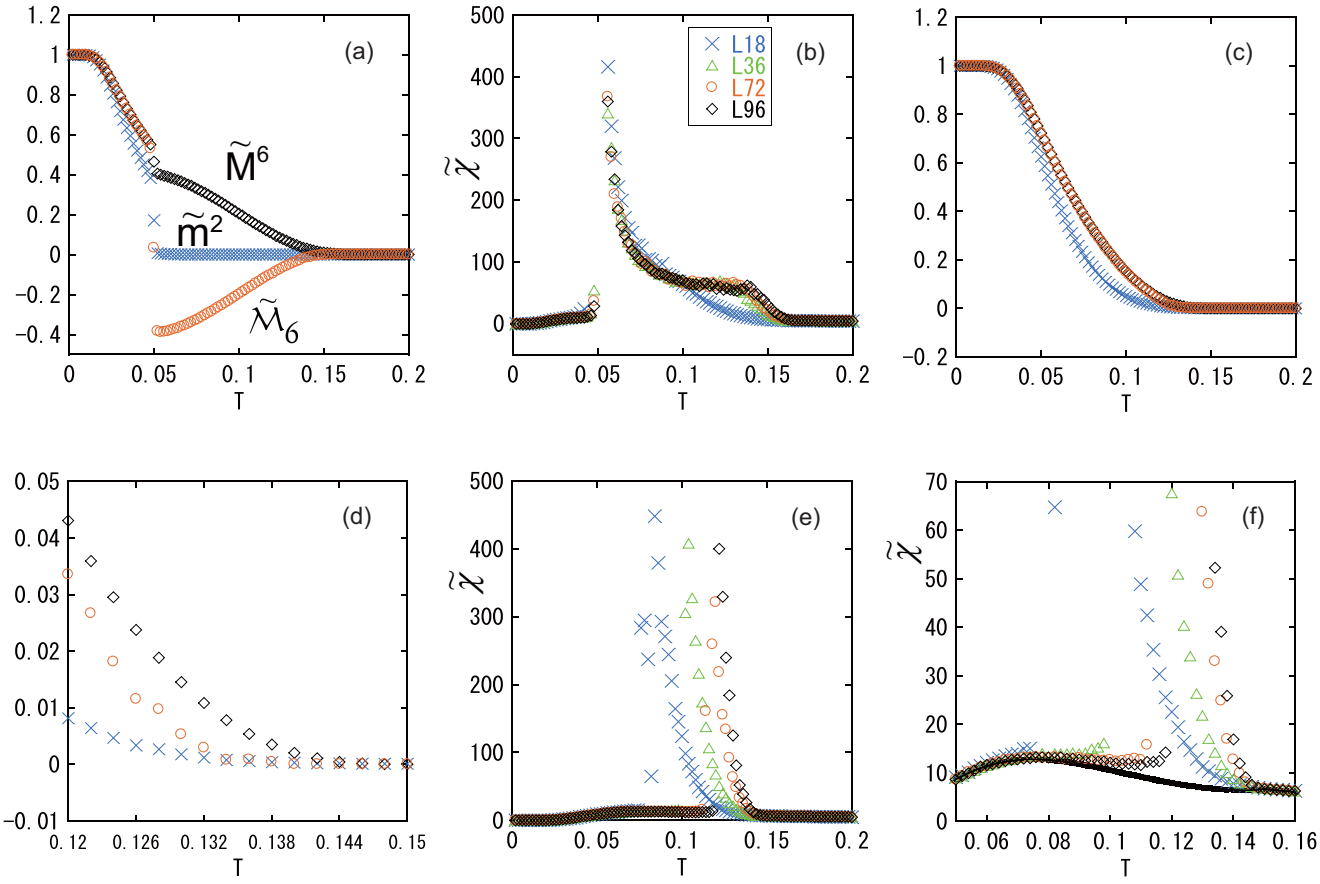

FIG. 12. (a) Temperature dependence of $\tilde{M}^6 = (\tilde{M}^2)^3$ (black diamonds), $\tilde{\mathcal{M}}_6$ (red circles), and $\tilde{m}^2$ (blue crosses) for $X = 0.15$ at $L = 96$. (b) $\tilde{\chi}$ for $X = 0.15$ at several system sizes. (c) Temperature dependence of $\tilde{M}^6$, $\tilde{\mathcal{M}}_6$, and $\tilde{m}^2$ for $X = 0.25$ at $L = 96$. (d) Magnified view of $\tilde{M}^6$, $\tilde{\mathcal{M}}_6$, and $\tilde{m}^2$ around the transition temperature for $X = 0.25$ at $L = 96$. (e) $\tilde{\chi}$ for $X = 0.25$ at several system sizes. (f) Comparison of $\tilde{\chi}$ for $X = 0.25$ between the thermodynamic limit (the MF theory; solid line) and finite systems.

The 3-FR phase should appear in the low-temperature region of the RG diagram of the long-range interaction models. Furthermore, the anomalous finite-size effect is seen in χ and $\tilde{\chi}$ for the order parameters m [Eq. (14)] and $\tilde{m}$ [Eq. (A1)] only in case II. (The susceptibilities for M [Eq. (15)] and $\tilde{M}$ [Eq. (A2)] diverge at T_N in cases I and II, which are not shown.) This aspect may be related to the fact that the PD phase has no magnetization and the ordering of the PD phase does not cause the enhancement of m. RG studies to explain this detail including the difference and similarity between the short-range and the long-range interaction models are a challenging problem for the future.

As mentioned in Sec. I, elastic interactions may realize effective infinite long-range sublattice interactions studied here, which is a very interesting and challenging future problem.

ACKNOWLEDGMENTS

The present work was supported by Grants-in-Aid for Scientific Research C (Grants No. 26400324 and No. 25400391) from MEXT of Japan and the Elements Strategy Initiative Center for Magnetic Materials under the outsourcing project of MEXT. The authors thank the Supercomputer Center, Institute for Solid State Physics, The University of Tokyo, for the use of the facilities.

APPENDIX A: FINITE-SIZE EFFECTS OF THE LONG-RANGE GENERALIZED SIX-STATE CLOCK MODEL

In this Appendix we investigate the finite-size effects of the LRG6SC model by use of the MC method. In the present model, the following quantities are defined as the order parameters:

$$\tilde{m}^2 = \frac{1}{N^2}\left\langle \left(\sum_{i=1}^{N} \cos 3\theta_i \right)^2 \right\rangle, \tag{A1}$$

which is regarded as the mean square value of "magnetization" (called magnetization hereafter). Corresponding to Eqs. (15), (16), and (17), we define

$$\tilde{M}^2 = \frac{1}{N^2}\left\langle \left\{ \sum_{i=1}^{N} \cos\theta_i \right\}^2 + \left\{ \sum_{i=1}^{N} \sin\theta_i \right\}^2 \right\rangle, \tag{A2}$$

where

$$\vec{\tilde{M}} = (\tilde{M}_x, \tilde{M}_y) = \left(\frac{1}{N}\sum_{i=1}^{N} \cos\theta_i,\ \frac{1}{N}\sum_{i=1}^{N} \sin\theta_i \right), \tag{A3}$$

and

$$\tilde{\mathcal{M}}_6 = \langle \mathrm{Re}[(\tilde{M}_x + i\tilde{M}_y)^6] \rangle. \tag{A4}$$

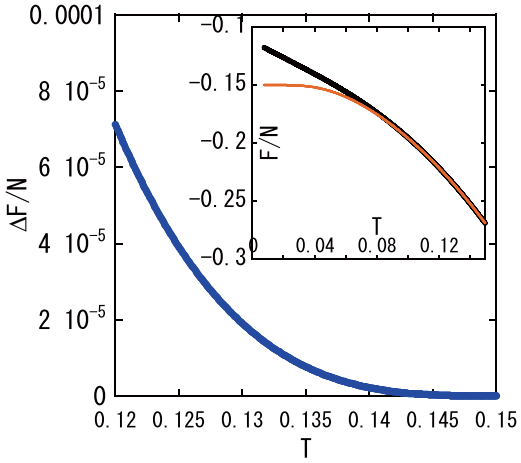

FIG. 13. Difference in the MF free energy density between the PD and the 2-FR phases in the LRG6SC model with $X = 0.25$. Insets: Free energy density of the PD phase (thick black line) and 2-FR phase (thin red line).

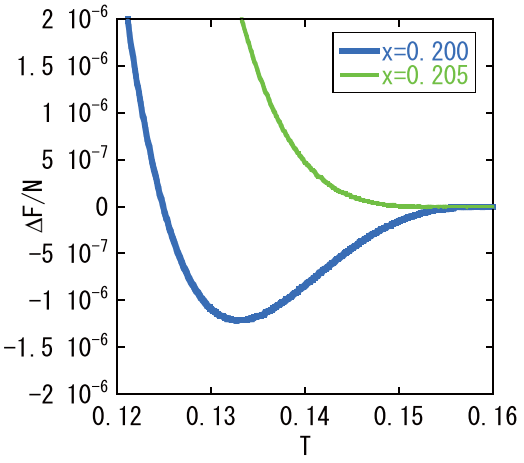

FIG. 14. Difference in the MF free energy density between the PD and the 2-FR phases in the LRG6SC model for $X = 0.200$ and $X = 0.205$. It leads to the critical value of X, i.e., $X_c \simeq 0.20$.

Here N is the number of sites ($N = L \times L$) in the triangular lattice (Fig. 1). We also define the magnetic susceptibility,

$$\tilde{\chi} = \frac{1}{NT}\left[\left\langle\left(\sum_{i=1}^{N}\cos 3\theta_i\right)^2\right\rangle - \left\langle\sum_{i=1}^{N}\cos 3\theta_i\right\rangle^2\right]. \quad \text{(A5)}$$

We plot the temperature dependence of $\tilde{M}^6$, $\tilde{\mathcal{M}}_6$, and $\tilde{m}^2$ for $X = 0.15$ at $L = 96$ in Fig. 12(a). Positive values of $\tilde{\mathcal{M}}_6$ are found at low temperatures, up to around $T = 0.05$, while negative values are found at higher temperatures, which suggests that the former is the 2-FR or 3-FR phase, while the latter is the PD phase. Figure 12(b) gives $\tilde{\chi}$ for $X = 0.15$ in several system sizes. A divergence of $\tilde{\chi}$ is seen at around $T = 0.05$, which is the phase transition point between the PD and the 3-FR phases. Thus, $X = 0.15$ belongs to case I.

We show the temperature dependence of $\tilde{M}^6$, $\tilde{\mathcal{M}}_6$, and $\tilde{m}^2$ for $X = 0.25$ at $L = 96$ in Figs. 12(c) and 12(d) (its magnification). The values of $\tilde{\mathcal{M}}_6$ in the ordered state are positive, suggesting the 2-FR phase. However, $\tilde{\chi}$ shows a divergencelike enhancement at around $T = 0.13$. Comparing $\tilde{\chi}$ between the infinite system (MF theory) and finite systems in Fig. 12(f), we find a difference similar to that in the LRTIAFF model. Thus, $X = 0.25$ belongs to case II.

Similarly to the case of LRTIAFF, $\tilde{\mathcal{M}}_6$ appears at a lower temperature than $\tilde{M}^6$, which should be attributed to the masslesslike-region scenario. We analyze the MF free energy structures of the PD and 2-FR phases in the same way as in the text. The difference in free energy density between the PD and the 2-FR phases, $\Delta F/N = (F_{\mathrm{PD}} - F_{2\text{-FR}})/N$, for $X = 0.25$ is depicted in Fig. 13. The insets show F_{PD}/N and $F_{2\text{-FR}}/N$. We find a small difference in $\Delta F/N$ when the temperature approaches the transition point. For $X = 0.25$, $\Delta F/N$ is about 10^{-5} at around $T = 0.13$. For $O(N) \simeq 10^4$, $\Delta F \simeq 10^{-1}$ and it is the order of the temperature.

Thus before the temperature decreases around $T = 0.13$, the free energies of both phases are regarded as the same and the two phases practically degenerate. The divergencelike enhancement of $\tilde{\chi}$ occurs via the same mechanism as in the LRTIAFF model.

APPENDIX B: CRITICAL VALUE OF X IN THE LONG-RANGE GENERALIZED SIX-STATE CLOCK MODEL

In the LRTIAFF model, $\alpha \simeq 0.8$ is the critical value for separating two kinds of transition processes, i.e., cases I and II. Here we study the corresponding critical value for X in the LRG6SC model. We analyze $\Delta F/N$ between $X = 0.15$ and $X = 0.25$ for the critical $X(X_c)$. In Fig. 14, $\Delta F/N$ is plotted as a function of the temperature for $X = 0.200$ and $X = 0.205$. The PD phase appears at $X = 0.205$ and it does not at $X = 0.200$, and we find $X_c \simeq 0.20$.

[1] H. T. Diep, *Frustrated Spin Systems* (World Scientific, Singapore, 2004).
[2] G. H. Wannier, Phys. Rev. **79**, 357 (1950); Phys. Rev. B **7**, 5017 (1973).
[3] H. Husimi and I. Shozi, Prog. Theor. Phys. **5**, 177 (1950); **5**, 341 (1950).
[4] R. M. F. Houttappel, Physica **16**, 425 (1950),
[5] M. Mekata and K. Adachi, J. Phys. Soc. Jpn. **44**, 806 (1978).
[6] M. Mekata, J. Phys. Soc. Jpn. **42**, 76 (1977).
[7] In the present study we define $\alpha > 0$, which corresponds to $-\alpha$ in Ref. [6].
[8] H. Takayama, K. Matsumoto, H. Kawahara, and K. Wada, J. Phys. Soc. Jpn. **52**, 2888 (1983).
[9] S. Fujiki, K. Shutoh, Y. Abe, and S. Katsura, J. Phys. Soc. Jpn. **52**, 1531 (1983).
[10] F. Matsubara and S. Inawashiro, J. Phys. Soc. Jpn. **53**, 4373 (1984); **56**, 2666 (1987).

[11] S. Miyashita, H. Kitatani, and Y. Kanada, J. Phys. Soc. Jpn. **60**, 1523 (1991).
[12] B. Mihura and D. P. Landau, Phys. Rev. Lett. **38**, 977 (1977).
[13] D. P. Landau, Phys. Rev. B **27**, 5604 (1983).
[14] M. Schick, J. S. Walker, and M. Wortis, Phys. Rev. B **16**, 2205 (1977).
[15] V. L. Berezinskii, Sov. Zhur. Eksp. Teor. Fiz. **59**, 907 (1970); **61**, 1144 (1971).
[16] J. M. Kosterlitz and D. J. Thouless, J. Phys. C **6**, 1181 (1973).
[17] H. W. J. Blöte and M. P. Nightingale, Phys. Rev. B **47**, 15046 (1993).
[18] J. V. José, L. P. Kadanoff, S. Kirkpatrick, and D. R. Nelson, Phys. Rev. B **16**, 1217 (1977).
[19] S. Elitzur, R. B. Pearson, and J. Shigemitsu, Phys. Rev. D **19**, 3698 (1979).
[20] J. L. Cardy, J. Phys. A: Math. Gen. **13**, 1507 (1980).
[21] A. N. Berker, G. S. Grest, C. M. Soukoulis, D. Blankschtein, and M. Ma, J. Appl. Phys. **55**, 2416 (1984).
[22] D. Blankschtein, M. Ma, A. N. Berker, G. S. Grest, and C. M. Soukoulis, Phys. Rev. B **29**, 5250 (1984).
[23] O. Koseki and F. Matsubara, J. Phys. Soc. Jpn. **69**, 1202 (2000).
[24] N. Todoroki and S. Miyashita, J. Phys. Soc. Jpn. **73**, 412 (2004).
[25] M. Oshikawa, Phys. Rev. B **61**, 3430 (2000).
[26] Edited by P. Gütlich and H. A. Goodwin, *Spin Crossover in Transition Metal Compounds I, II, III* (Springer, Berlin, 2004).
[27] M. A. Halcrow (ed.), *Spin-Crossover Materials: Properties and Applications* (John Wiley & Sons, Chichester, UK, 2013).
[28] O. Kahn and C. Jay Martinez, Science **279**, 44 (1998).
[29] A. Hauser, J. Jeftić, H. Romstedt, R. Hinek, and H. Spiering, Coord. Chem. Rev. **190-192**, 471 (1999).
[30] J. F. Letard, P. Guionneau and L. Goux-Capes, Top. Curr. Chem. **235**, 221 (2004).
[31] S. Kimura, Y. Narumi, K. Kindo, M. Nakano, and G.-e. Matsubayashi, Phys. Rev. B **72**, 064448 (2005).
[32] S. Pillet, V. Legrand, M. Souhassou, and C. Lecomte, Phys. Rev. B **74**, 140101(R) (2006).
[33] K. Ichiyanagi, J. Hebert, L. Toupet, H. Cailleau, P. Guionneau, J.-F. Létard, and E. Collet, Phys. Rev. B **73**, 060408(R) (2006).
[34] M. Lorenc, J. Hébert, N. Moisan, E. Trzop, M. Servol, M. Buron-Le Cointe, H. Cailleau, M. L. Boillot, E. Pontecorvo, M. Wulff, S. Koshihara, and E. Collet, Phys. Rev. Lett. **103**, 028301 (2009).
[35] H. Watanabe, H. Hirori, G. Molnár, A Bousseksou, and K. Tanaka, Phys. Rev. B **79**, 180405(R) (2009).
[36] N. Bréfuel, H. Watanabe, L. Toupet, Jérémy Come, N. Matsumoto, E. Collet, K. Tanaka, and J.-P. Tuchagues, Angew. Chem. Int. Ed. **48**, 9304 (2009).
[37] C. Chong, F. Varret, and K. Boukeddaden, J. Phys. Chem. B **114**, 1975 (2010).
[38] A. Bousseksou, G. Molnar, L. Salmon, and W. Nicolazzi, Chem. Soc. Rev. **40**, 3313 (2011).
[39] A. Slimani, F. Varret, K. Boukheddaden, C. Chong, H. Mishra, J. G. Haasnoot, and S. Pillet, Phys. Rev. B **84**, 094442 (2011).
[40] R. Bertoni, M. Lorenc, H. Cailleau, A. Tissot, J. Laisney, M.-L. Boillot, L. Stoleriu, A. Stancu, C. Enachescu, and E. Collet, Nat. Mater. **15**, 606 (2016).
[41] H. Spiering, E. Meissner, H. Koppen, E. W. Muller, and P. Gütlich, Chem. Phys. **68**, 65 (1982).
[42] P. Adler, L. Wiehl, E. Meißner, C. P. Köhler, H. Spiering, and P. Gütlich, J. Phys. Chem. Solids **48**, 517 (1987).
[43] N. Willenbacher and H. Spiering. J. Phys. C: Solid State Phys. **21**, 1423 (1988).
[44] M. Nishino, K. Boukheddaden, Y. Konishi, and S. Miyashita, Phys. Rev. Lett. **98**, 247203 (2007).
[45] S. Miyashita, Y. Konishi, M. Nishino, H. Tokoro, and P. A. Rikvold, Phys. Rev. B **77**, 014105 (2008).
[46] W. Nicolazzi, S. Pillet, and C. Lecomte, Phys. Rev. B **78**, 174401 (2008).
[47] M. Nishino, K. Boukheddaden, and S. Miyashita, Phys. Rev. B **79**, 012409 (2009).
[48] C. Enachescu, L. Stoleriu, A. Stancu and A. Hauser, Phys. Rev. Lett. **102**, 257204 (2009).
[49] C. Enachescu, M. Nishino, S. Miyashita, A. Hauser, A. Stancu, and L. Stoleriu, Europhys. Lett. **91**, 27003 (2010).
[50] C. Enachescu, M. Nishino, S. Miyashita, L. Stoleriu, and A. Stancu, Phys. Rev. B **86**, 054114 (2012).
[51] T. Nakada, T. Mori, S. Miyashita, M. Nishino, S. Todo, W. Nicolazzi, and P. A. Rikvold, Phys. Rev. B **85**, 054408 (2012).
[52] M. Nishino and S. Miyashita, Phys. Rev. B **88**, 014108 (2013).
[53] A. Slimani, K. Boukheddaden, F. Varret, H. Oubouchou, M. Nishino, and S. Miyashita, Phys. Rev. B **87**, 014111 (2013).
[54] M. Nishino and S. Miyashita, Phys. Rev. B **92**, 184404 (2015).
[55] S. Cobo, G. Molnár, J. A. Real, and A. Bousseksou, Angew. Chem. Int. Ed. **45**, 5786 (2006).
[56] E. Coronado, J. R. Galán-Mascarós, M. Monrabal-Capilla, J. García-Martínez, and P. Pardo-Ibañez, Adv. Mater. **19**, 1359 (2007).
[57] G. Molnár, S. Cobo, J. A. Real, F. Carcenac, E. Daran, C. Vieu, and A. Bousseksou, Adv. Mater. **19**, 2163 (2007).
[58] F. Volatron, L. Catala, E. Rivière, A. Gloter, O. Stéphan, and T. Mallah, Inorg. Chem. **47**, 6584 (2008).
[59] I. Boldog, A. B. Gaspar, V. Martínez, P. Pardo-Ibañez, V. Ksenofontov, A. Bhattacharjee, P. Gütlich, and J. A. Real, Angew. Chem. Int. Ed. **47**, 6433 (2008).
[60] We calculated the difference in the MF free energies of the 2-FR vs the PD phases as a function of the temperature T, where the temperature step was taken as $\Delta T = 0.001$. We obtained $0.799 < \alpha_C < 0.800$ from this estimation.
[61] F. Y. Wu, Rev. Mod. Phys. **54**, 235 (1982).
[62] S. Miyashita, J. Phys. Soc. Jpn. **66**, 3411 (1997).
[63] T. Okubo, K. Oshikawa, H. Watanabe, and N. Kawashima, Phys. Rev. B **91**, 174417 (2015).
[64] F. Léonard and B. Delamotte, Phys. Rev. Lett. **115**, 200601 (2015).